Available online at www.sciencedirect.com
ScienceDirect
International Journal of Heat and Mass Transfer 51 (2008) 4095–4108
International Journal of HEAT and MASS TRANSFER
www.elsevier.com/locate/ijhmt

Rotating Rayleigh–Bénard convection under the influence of transverse magnetic field

Hirdesh Varshney, Mirza Faisal Baig *

Department of Mechanical Engineering, A.M.U., Aligarh 202 002, India

Received 19 January 2007; received in revised form 13 August 2007
Available online 7 March 2008

Abstract

In the present numerical study the effect of constant transverse magnetic field on convection of low Prandtl number liquid metal rotating in a cubical cavity with an aspect-ratio of 8:8:1 has been investigated. The bottom wall is heated while the top-wall is cooled and all the other walls are kept thermally insulated. The governing equations of mass, momentum, energy and magneto-hydrodynamic for a frame rotating with the enclosure, subject to Boussinesq approximation applied to gravity and centrifugal force terms, have been solved on a collocated grid using a semi-implicit finite difference method. The simulations have been carried out for liquid metal flows having a fixed Prandtl number $Pr = 0.01$, Rayleigh number $Ra = 10^7$, and magnetic Prandtl number $Pm = 4.0 \times 10^{-4}$ while Chandrasekhar number Q varies from 5.0625×10^4 to 1.21×10^6 and non-dimensional rotation rate Ω is varied from zero to 10^5.

The increase in strength of transverse magnetic field (from $Q_l = 5.0625 \times 10^4$ to $Q_h = 1.21 \times 10^6$) till $Q \simeq Ta$ leads to slight increase in convective heat transfer as well as formation of two-dimensional coherent structures aligned along the direction of magnetic field. For cases pertaining to $Q < Ta$ the two-dimensionality of the flow breaks down and the rolls distort in their alignment which leads to decrease in magnitude of vertical heat transfer. For cases where $Q \ll Ta$, the increased Coriolis forces lead to generation of large-scale circulation which forms a large cylindrical rotating column of fluid in consonance with Taylor–Proudman theorem. On increasing the strength of magnetic field the component of rms velocity in the direction of magnetic field gets suppressed while there is increase in other two components.

Keywords: Rotating Rayleigh–Bénard convection; Transverse magnetic field; Two-dimensional coherent structures; Coriolis forces

1. Introduction

The turbulent Rayleigh–Bénard convection is primarily due to the instability of Boussinesq fluid. The turbulent convection with rotation is an important phenomena in many industrial applications as well as in astrophysical and geophysical flows. Further introduction of magnetic field makes the flow more complex and can have profound effect on the convection. In the present paper we focus on the behavior of flow of an electrically conducting Boussinesq liquid metal in a rotating rectangular enclosure heated from bottom while being subjected to an applied magnetic field transverse to the temperature gradient.

The controlling non-dimensional parameters in rotating magneto-convection are

- Rayleigh number $Ra = \frac{\alpha g H^3 \triangle T}{\nu \kappa}$ is the ratio of buoyancy forces to viscous forces and represents the driving force of convection where α is the thermal expansion coefficient, g is the magnitude of the acceleration due to gravity, ν is the kinematic viscosity and $\kappa = \lambda/\rho c_p$ is the thermal diffusivity with the thermal conductivity λ, density ρ and the specific heat capacity c_p.
- Chandrasekhar number $Q = Ha^2 = \frac{\sigma H^2 B_\circ^2}{\rho_\circ \nu}$ is the square of the Hartmann number Ha and represents the ratio of Lorentz forces $F_L = \mathbf{j} \times \mathbf{B}$, that are produced by the

* Corresponding author. Tel.: +91 9897517071.
E-mail address: drmfbaig@yahoo.co.uk (M.F. Baig).

0017-9310/$ - see front matter © 2008 Elsevier Ltd. All rights reserved.
doi:10.1016/j.ijheatmasstransfer.2007.11.046

Nomenclature

B, L and H breadth, length and height of flow domain (m)
g acceleration magnitude due to gravity (m/s^2)
$\overline{Nu}$ spaced-averaged Nusselt number
Pr Prandtl number v/κ
Ra Rayleigh number $(\alpha g H^3 \Delta T)/(v\kappa)$
$Ra_w = \frac{(\Omega_D^2 H)\alpha H^3 \triangle T}{v\kappa}$
$Q = Ha^2$ Chandrasekhar number, $\frac{\sigma H^2 B_\circ^2}{\rho_\circ v}$
Ta Taylor number, $\frac{\Omega_D^2 H^4}{v^2}$
Pm Magnetic Prandtl number, $\frac{v}{v_h}$
T dimensional temperature (K)
t non-dimensional time
T_c initial fluid temperature (K)
$\mathbf{V}$ dimensional velocity vector (m/s)
$\mathbf{u}$ dimensionless velocity vector
$\overline{u}, \overline{v}, \overline{w}$ dimensionless mean velocities in x, y and z-directions
X, Y, Z dimensional coordinate system (m)
Ω_D dimensional angular rotation speed (rad/s)
$\mathbf{B}$ dimensionless magnetic field vector
$\mathbf{j}$ dimensionless current density
C_p specific heat at constant pressure $\frac{J}{kg\ K}$

Greek symbols
$\Gamma = L/H = B/H$ aspect-ratio of enclosure.
Θ non-dimensional temperature, $(T - T_c)/\Delta T$
$\overline{\Theta}$ non-dimensional mean temperature
$\rho_\circ$ reference density of fluid (kg/m^3)
Δt non-dimensional time-step
ΔT temperature difference between hot and cold walls (K)
v kinematic viscosity ($\frac{m^2}{s}$)
v_h magnetic diffusivity ($\frac{m^2}{s}$)
α coefficient of thermal expansion (K^{-1})
κ thermal diffusivity (m^2/s)
σ electrical conductivity, $(\text{ohm} - \text{m})^{-1}$

Acronyms
CGSTAB conjugate gradient stabilized
RBC Rayleigh–Bénard convection
SOR successive-over relaxation

interaction of the current density $\mathbf{j}$ with the magnetic field $\mathbf{B}$ to the viscous forces. Here σ is the electrical conductivity, $B_\circ$ the magnitude of externally imposed magnetic field.

- Taylor number $Ta = \frac{\Omega_D^2 H^4}{v^2}$ is the squared ratio of Coriolis forces to viscous forces. Here Ω_D is the dimensional angular velocity about the vertical axis.
- Rotational Rayliegh number $Ra_w = \frac{(\Omega_D^2 H)\alpha H^3 \triangle T}{v\kappa}$ which is the ratio of rotational buoyancy (centrifugal force) to viscous force.
- Prandtl number $Pr = \frac{v}{\kappa}$ is the ratio of the viscous and the thermal diffusion and characterizes diffusive properties of the fluid.
- Magnetic Prandtl number $Pm = \frac{v}{v_h}$ is the ratio of the viscous to the magnetic diffusion. The induced magnetic will be small for lower value of Pm and larger for larger value of Pm.
- Magnetic Reynolds number $Re_m = \frac{Pm}{Pr}$ is the ratio of thermal to magnetic diffusion. If $Re_m \ll 1$, then the magnetic diffusion is the dominant process and the magnetic field distortion will be negligible. Thermal convection in the bounded regions also depends on the aspect-ratio $\Gamma = \frac{L}{H} = \frac{B}{H}$.

Some of the numerical and experimental works that have been done till date to study the rotating or non-rotating magneto-convection in rectangular or cylindrical enclosures are enumerated below.

Lehnert and Little [1] experimentally studied the effect of inhomogeneity and obliquity of a magnetic field in inhibiting convection. In their results they stated that when the direction of imposed magnetic field is different from the vertical, only the component of magnetic field in the direction of vertical is effective. Also for the case of horizontal magnetic field, there is no discernible effect in inhibiting convection even though the field was five times to that necessary to suppress convection, if acting in the vertical direction. Moreover, the pattern of convective rolls is in the form of elongated cells extending across the entire vessel parallel to the magnetic field.

Ozoe and Okada [2] numerically studied the effect of the direction of external magnetic field on natural convection in a cubical enclosure. Three-dimensional conservation equations for natural convection of molten silicon in a cubical enclosure heated from one vertical side-wall and cooled from an opposing wall are numerically solved under three different external magnetic fields either in the x-, y-, or z- directions for $Ra = 10^6$ and 10^7, $Ha = 0 - 500$ at a fixed $Pr = 0.054$. They found that the external magnetic field is most effective in suppressing the convection when applied perpendicular to the heated vertical wall. It is least effective when the magnetic field is horizontal and parallel to the heated vertical wall.

Juel et al. [3] experimentally and numerically studied the effects of a steady transverse magnetic field on side-wall convection in molten gallium inside a rectangular cavity of square cross-section with an aspect-ratio $\Gamma = l/h = 4$. They found that the flow is restricted to two-dimensions and the oscillations due to large temperature gradients can be suppressed effectively by the magnetic field.

Ben Hadid and Henry [4] numerically studied the convection in a cubical enclosure under the action of imposed ver-

tical and transverse magnetic fields in a $4 \times 1 \times 1$ rectangular cavity with constant horizontal temperature gradient. They found that in case of a vertical magnetic field at relatively small Hartmann number $Ha \geqslant 10$, the magnetic field is primarily associated with breaking of the average flow in the melt, but at sufficiently large $Ha \geqslant 100$ the flow becomes unidirectional over a large part of the cavity with a quiescent core region surrounded at top and bottom by Hartmann boundary layers and by parallel layers at the vertical sidewalls. For the case of transverse magnetic field they reported a decrease in the vertical velocity, but only at larger values of Ha, i.e. for $Ha \geqslant 50$ in comparison to the vertical magnetic field ($Ha \geqslant 10$). The comparison of the maxima of vertical velocity indicates that the magnetic damping is most efficient for the case of vertical magnetic field.

Aurnou and Olson [5] experimentally measured heat transfer for liquid gallium ($Pr = 0.023$), subject to the combined action of rotation and a uniform vertical magnetic field in a rectangular cavity of size $15.2 \times 15.2 \times 3.8$ cm. They found that for rotating magneto-convection, the convective heat transfer is inhibited by rotation for supercritical Taylor number $Ta > 10^4$.

Burr and Muller [6] studied the Rayleigh–Bénard convection in a liquid metal layers under the influence of a horizontal magnetic field. In their study they report that vorticity lines tend to become aligned with the magnetic field and due to this the flow properties like convective heat flux are governed by opposing mechanisms of Julian dissipation which tries to reduce convection and two-dimensional coherent structures which promote convective heat transport.

Most of the numerical and experimental works reviewed above are concerned with the effect of magnetic field on non-rotating convection except the work of Aurnou and Olson [5]. The main aim of our study is to analyze the effect of magnetic field and rotation, when applied orthogonal to each other, on the dynamics of the flow and convection by exploring the seven-dimensional parametric space on varying two independent parameters namely Ta and Q. Further, we would like to investigate the formation of coherent structures in rotating magneto-convection and how they influence the heat and momentum transport. Besides this, we also want to determine the effect of rotation with transverse magnetic field on statistics of dynamical variables.

The present work involves a numerical study of three-dimensional rotating magneto-convection in a moderately large aspect-ratio (8:8:1) enclosure, rotating about a vertical axis passing through its center of gravity. In Fig. 1 the flow problem under consideration is sketched. Liquid metal is confined in a rectangular enclosure with no-slip boundary conditions applied at all the walls. The bottom wall is heated and the upper one is cooled so that a temperature difference ΔT with an associated heat flux $\mathbf{q}$ is maintained across the gap. All other walls are thermally insulated. A homogeneous magnetic field $\mathbf{B}$ in y-direction is imposed in transverse direction to the applied temperature difference. The simulations have been carried out

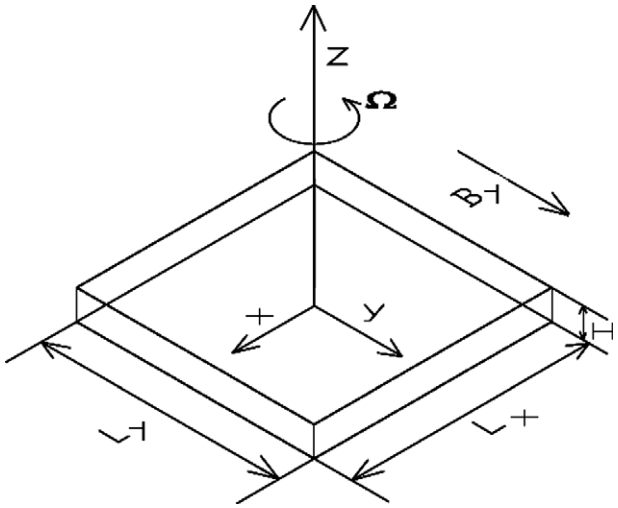

Fig. 1. Schematic diagram of geometry of the domain.

for liquid metal flows having a fixed Prandtl number, $Pr = 0.01$, Rayleigh number, $Ra = 10^7$ and magnetic Prandtl number, $Pm = 4.0 \times 10^{-4}$ while Chandrasekhar number Q and Taylor number Ta are varied through dimensional rotation rate Ω_D. To stringently maintain the Bousinessq condition, the ratio of $\frac{Ra_w}{Ta}$ is kept as 10^{-3} for all the simulations.

2. Mathematical model

The basic equations used in the simulation of rotating flow subjected to magnetic field are the incompressible 3D Navier-Stokes equations with inclusion of Lorentz, Coriolis and rotational buoyancy (Centrifugal) forces, energy equation and the magneto-hydrodynamic equations. Boussinesq approximation, i.e. linear variation of density with small temperature difference has been considered for both the gravity and centrifugal force terms [7,8]. The conservation equations are made dimensionless using length scale (H), time scale (H^2/κ), velocity scale (κ/H), pressure scale ($\rho_o \kappa^2/H^2$), temperature scale ($\Theta = (T - T_c)/\Delta T$) and ($\nu/H^2$) scale for rotation rate. Using these reference scales, the governing equations may be written as

Conservation of mass

$$\nabla \cdot \mathbf{u} = 0 \tag{1}$$

Conservation of momentum in rotating coordinate frame

$$\frac{\partial \mathbf{u}}{\partial t} + \mathbf{u} \cdot \nabla \mathbf{u} = -\nabla p + Pr \nabla^2 \mathbf{u} + (2Ta^{0.5} Prv - Ra_w x Pr\Theta)\hat{i} + (-2Ta^{0.5} Pru - Ra_w y Pr\Theta)\hat{j} + RaPr\Theta\hat{k} + \frac{Pr^2}{Pm} Q[\nabla \times \mathbf{B} \times \mathbf{B}] \tag{2}$$

Conservation of energy

$$\left(\frac{\partial \Theta}{\partial t} + \mathbf{u} \cdot \nabla \Theta\right) = \nabla^2 \Theta + \frac{Q}{Ra}\left(\frac{Pr^2}{Pm}\right)\frac{\alpha g H}{c_p}(\nabla \times \mathbf{B})^2 \tag{3}$$

Magneto-hydrodynamics

$$\frac{\partial \mathbf{B}}{\partial t} + \mathbf{u}\cdot\nabla\mathbf{B} = (\mathbf{B}\cdot\nabla)\mathbf{u} + \frac{1}{Re_m}\nabla^2\mathbf{B} \tag{4}$$

Initially the fluid is supposed to be in the quiescent state ($u = 0,\ v = 0,\ w = 0$) with respect to the rotating frame of reference at isothermal conditions $T = T_c$, i.e. $\Theta = 0$. No-slip conditions for velocity components at the solid boundaries, i.e. $u = v = w = 0$ are enforced. The thermal boundary conditions are $\partial\Theta/\partial x = 0$ at $x = \pm L/2$, $\partial\Theta/\partial y = 0$ at $y = \pm B/2$, $\Theta = 1$ at $z = -H/2$ and $\Theta = 0$ at $z = H/2$. The magneto-hydrodynamic initial conditions are taken as $B_y = 1.0$, $B_x = B_z = 0$, while the boundary conditions are

$$\partial \mathbf{B}_n/\partial n = 0$$

in order to satisfy continuity on the interface between the fluid and the walls. The walls of the cavity are assumed to be electrically insulated hence $\mathbf{j}_n = 0$ at all the walls [9].

The non-dimensional heat transfer across the fluid layer is given in terms of the space-averaged Nusselt number at both the cold and hot walls has been calculated using the relation

$$Nu = -\frac{1}{L\times B}\int_{-L/2}^{L/2}\int_{-B/2}^{B/2}\left(\frac{\partial\Theta}{\partial z}\right)\mathrm{d}x\mathrm{d}y$$

3. Numerical scheme and validation

Eqs. (1)–(4) are solved in time using second-order explicit Adam-Bashforth integration scheme. The convective non-linear terms are discretized using Taylor-series based upwind scheme. First-order accurate upwind scheme is used at points adjacent to the domain boundaries while third-order accurate upwind scheme is used in the interior domain. Viscous and thermal diffusion terms as well as pressure terms present in the momentum and energy equations are discretized using second-order accurate central differencing scheme. The details of the numerical scheme used to solve the equations has been explained in greater detail in Nadeem and Baig [10].

We validate our numerical scheme with Lee and Lin [11] for differentially heated rotating convection, initially without considering magnetic field. The results obtained are quite close to the one obtained by Lee and Lin [11] as shown in Tables 1 and 2. We feel that our results on a similar grid of $30 \times 30 \times 30$ are more accurate, as the pressure Poisson solver in our case is based on CGSTAB technique while Lee and Lin [11] used SOR technique and hence had to use a much higher residual norm of 10^{-4} compared to our norm of 10^{-11}. The above validation was to check the efficiency of numerical scheme for rotating convection. To check the accuracy of the scheme for solving magneto-hydrodynamics equations, we also validate our results with experimental results of Aurnou and Olson [5] for Rayleigh–Bénard convection with vertical magnetic field. For a cubical cavity of aspect-ratio 6:6:1, using a coarse mesh of $31 \times 31 \times 19$ at $Ra = 4 \times 10^4$, $Pr = 0.023$, $Pm = 1.5 \times 10^{-6}$ and Chandrasekhar number $Q = 1210$, we found the mean Nusselt number on both the walls ($Nu = 1.26$) to be in excellent agreement with experimental values of $Nu = 1.25$.

Table 1
Comparison of the maximum local velocities at $Ra = 10^2$, $Ta = 10^2$, and $Ra_w = 10^6$

Time (t)	$\lvert u_{max}\rvert$	$\lvert u_{max}\rvert$	$\lvert v_{max}\rvert$	$\lvert v_{max}\rvert$	$\lvert w_{max}\rvert$	$\lvert w_{max}\rvert$
	Lee and Lin [11]	Present work	Lee and Lin [11]	Present work	Lee and Lin [11]	Present work
0.05	130.54	127.96	94.24	91.19	22.08	21.23
0.10	122.08	122.25	90.42	88.65	21.84	20.77
0.15	119.48	120.57	89.15	88.21	21.75	20.91
0.20	118.74	120.24	89.15	88.09	21.73	20.89
S.S.	118.56	120.15	89.08	88.06	21.73	20.89

Table 2
Comparison of the average Nusselt number at $Ra = 10^2$, $Ta = 10^2$, and $Ra_w = 10^6$ at the bottom heated wall

Time (t)	Nu at $x = -0.5$	Nu at $x = -0.5$
	Lee and Lin [11]	Present work
0.05	4.773	4.525
0.10	4.182	4.026
0.15	4.020	3.955
0.20	3.971	3.934
S. S.	3.956	3.92

Regarding grid independence, we simulated rotating magneto-convection on a geometrical progression based collocated grid of $141 \times 141 \times 61$. We found that integral parameters such as mean Nusselt number $\overline{Nu}$ changed by less than 4% compared to the coarse grid. Moreover, the global maximum velocities u, v and w changed by less than 4%. Hence in order to cut down the computational time, we ran all our simulation cases on a comparatively coarser grid of $71 \times 71 \times 31$. The spacing of grid is based on geometric progression series with the minimum grid spacing being 0.005 near the boundary for all the spatial directions.

4. Results and discussion

The present study focuses on the combined effect of transverse magnetic field and rotation on the flow dynamics and heat transfer. To analyze the flow characteristics we have performed eight numerical simulations by varying Chandrasekhar number Q from 5.0625×10^4 to 1.21×10^6 for four rotational rates namely 0, 10^3, 5×10^3 and 10^5 keeping $Ra = 10^7$, $Pr = 0.01$ and $Pm = 4 \times 10^{-4}$ as constant. The Taylor number Ta varies from 0 to 10^{10} corresponding to the rotational speeds. The rotational Rayliegh number Ra_w is computed such that the ratio of $\frac{Ra_w}{Ta}$ remains constant as 10^{-3}. This ratio stringently satisfies Boussinesq approximation for all the eight simulations. The value of Rayleigh number taken in our study is well above the critical Rayleigh number, both for non-rotating as well as rotating magneto-convection cases and this ensures unstable convection. The results we obtain from

simulations have been classified on the basis of either dominance of Lorentz or Coriolis force. Broadly this yields five cases satisfying three conditions namely $Q > Ta$, $Q \simeq Ta$ and $Q \ll Ta$.

4.1. Spatial flow analysis

The transverse magnetic field produces strong anisotropy which leads to tendency of vorticity lines to align with the direction of magnetic field. For the first simulation at lower magnetic field strength ($Q < Ta$) corresponding to $Q_l = 5.0625 \times 10^4$ and zero-rotation, i.e. $Ta = 0$, it is observed that multiple small-size rolls in the transverse plane perpendicular to the applied magnetic field (see Fig. 2b) and there is a weak alignment of these rolls parallel to the magnetic field (see Fig. 2a). The thermal field shows multiple rising and descending isotherms weakly aligned along the direction of magnetic field (see Fig. 2c and d).

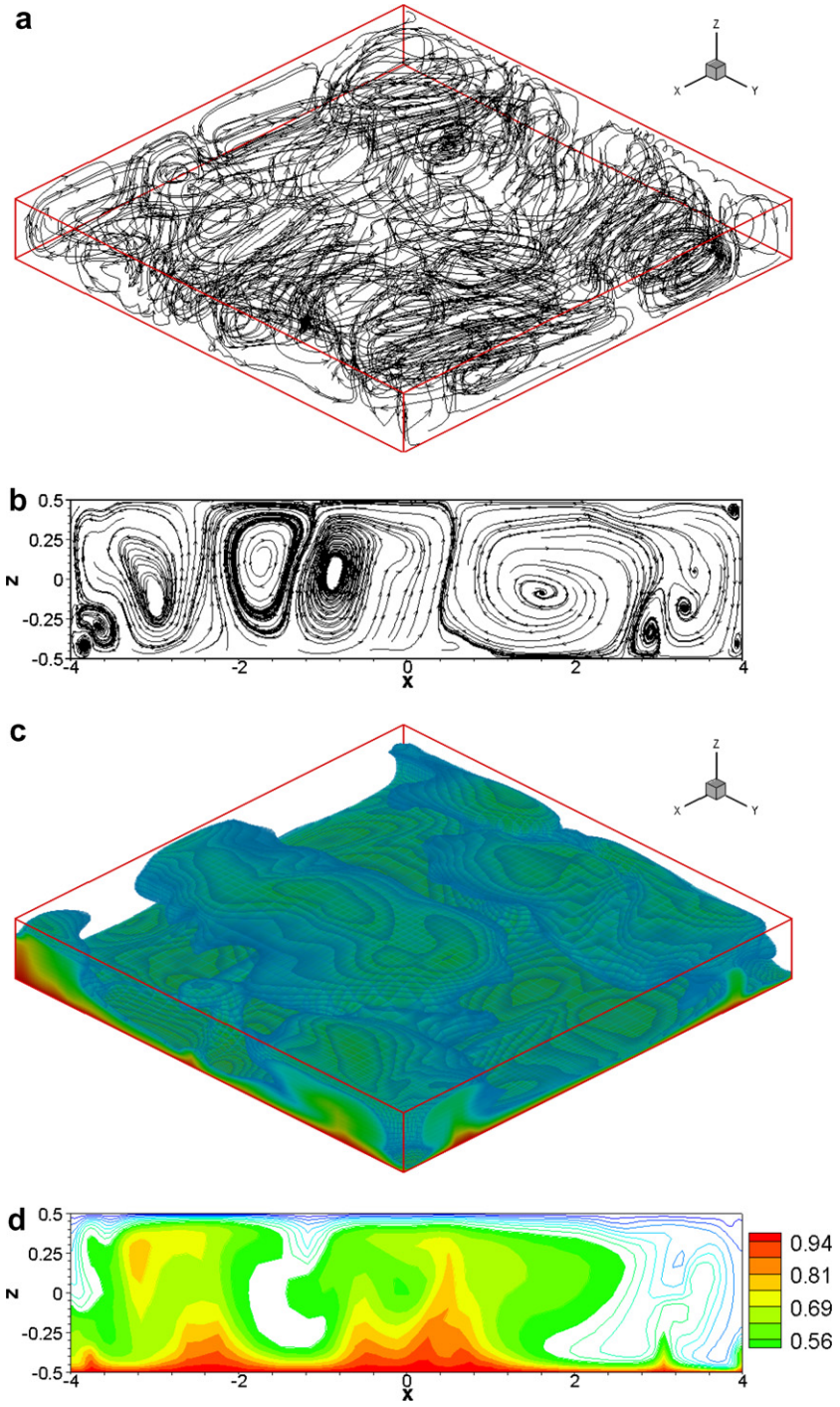

Fig. 2. Streamline plots of (a) 3D flow structures for $Q > Ta$, $Q_l = 5.0625 \times 10^4$ and $Ta = 0$, (b) 2D flow structures in central xz-plane. Isotherms showing (c) 3D thermal structures and (d) 2D thermal structures in central xz-plane.

As the strength of the magnetic field is increased such that $Q_h = 1.21 \times 10^6$ and $Ta = 0$, 5 large circular rolls stretched in the direction of applied magnetic field are found as shown in Fig. 3a and b. These rolls are representative of two-dimensional coherent structures as reported in the findings of Burr and Muller [6]. While the thermal structures (see isotherms in Fig. 3c and d) with lower cutoff value of isotherms set at 0.5 show a number of rising and descending plumes again aligned parallel to the magnetic field.

For the case pertaining to $Q_l = 5.0625 \times 10^4$ and $Ta = 10^6$, there is formation of two large-rolls in the xz-plane and the 3D-plot shows these rolls are weakly aligned in the transverse y-direction. On increasing the strength of magnetic field at same Ta, when the applied magnetic field and Coriolis force are of comparable magnitude, i.e. $Q \simeq Ta$ ($Q_h = 1.21 \times 10^6$, $Ta = 10^6$), the dynamics of flow changes such that the rolls observed for the previous case, now split and form four large-rolls elongated in the direc-

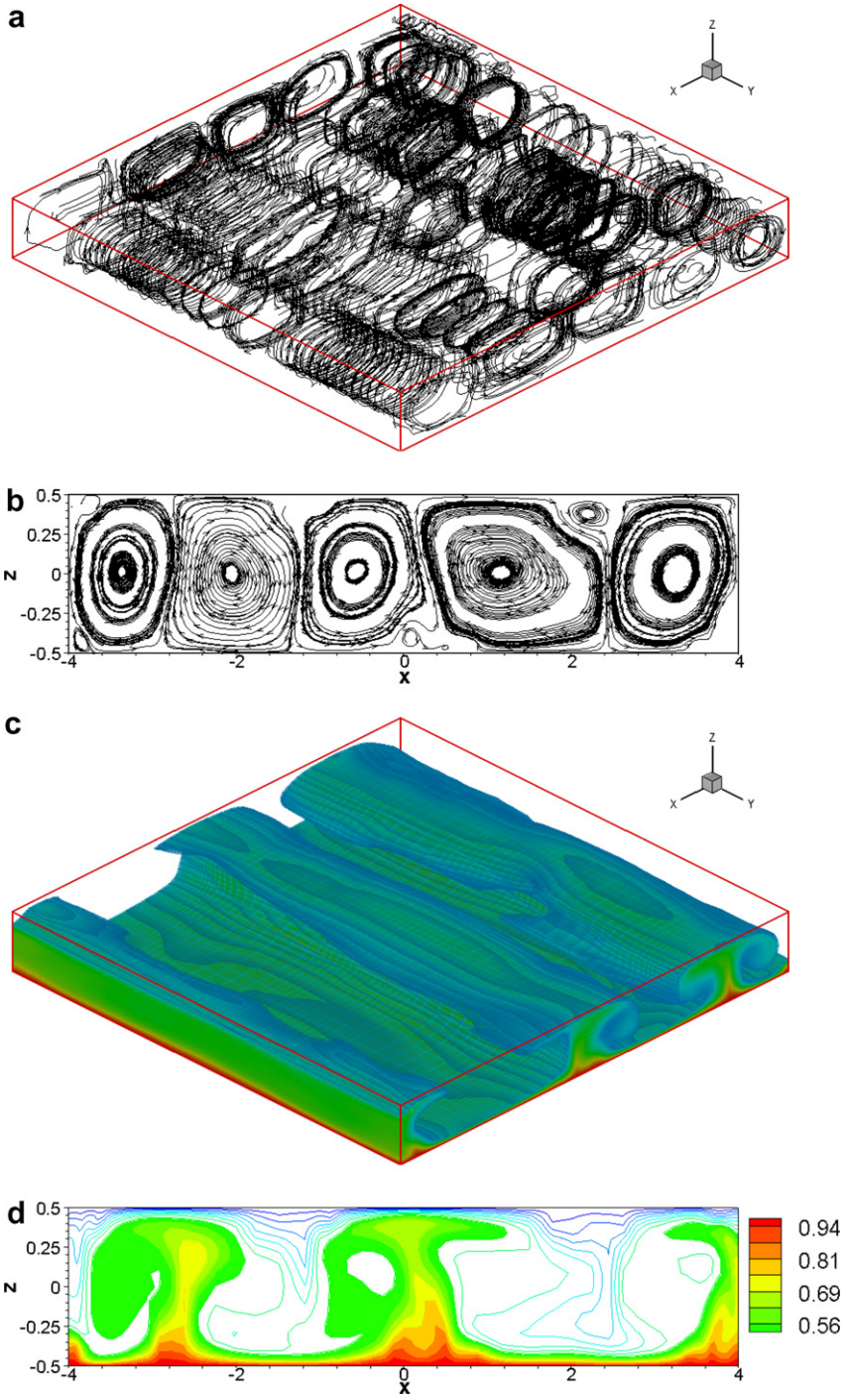

Fig. 3. Streamline plots of (a) 3D flow structures for $Q > Ta$, $Q_h = 1.21 \times 10^6$ and $Ta = 0$, (b) 2D flow structures in central xz-plane. Isotherms showing (c) 3D thermal structures and (d) 2D thermal structures in central xz-plane.

tion of magnetic field (see Fig. 4a and b). It suggests that the transverse magnetic field with comparable Coriolis force leads to strong two-dimensional turbulence transverse to the applied magnetic field. A similar phenomenon is observed in thermal flow field as shown in Fig. 4c and d. Here again the individual plumes found for the case $Q > Ta$ merge together to form two rising and two descending large-size plumes which are elongated parallel to the direction of magnetic field.

When the Coriolis force is the dominant force, i.e. $Q < Ta$, for the case $Q_h = 1.21 \times 10^6$ and $Ta = 2.5 \times 10^7$, the strong two-dimensionality is broken by the Coriolis force and the ensuing circulation skews the directional alignment of rolls (see Fig. 5a) while in the transverse central xz-plane larger number of rolls are generated as shown in Fig. 5b. The thermal flow field shows two large-sized ascending and two small-sized descending plumes as shown in Fig. 5c and d.

When the rotation rate is increased to $Ta = 10^{10}$, i.e. $Q \ll Ta$ corresponding to $Q_h = 1.21 \times 10^6$ and $Ta = 10^{10}$, the dominance of Coriolis force generates a strong circulation which in turn forms a large cylindrical column of fluid

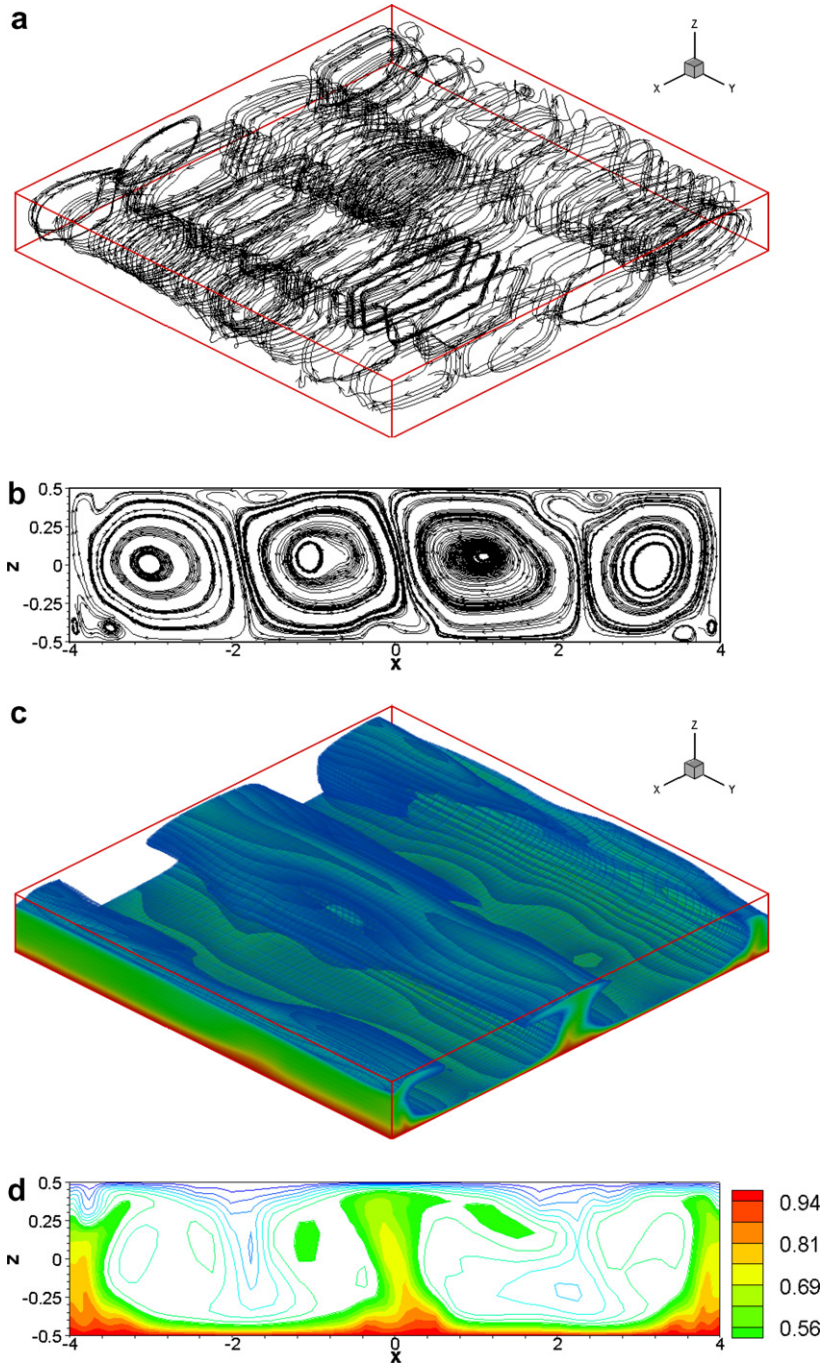

Fig. 4. Streamline plots of (a) 3D flow structures for $Q \simeq Ta$, $Q_h = 1.21 \times 10^6$ and $Ta = 10^6$, (b) 2D flow structures in central xz-plane. Isotherms showing (c) 3D thermal structures and (d) 2D thermal structures in central xz-plane.

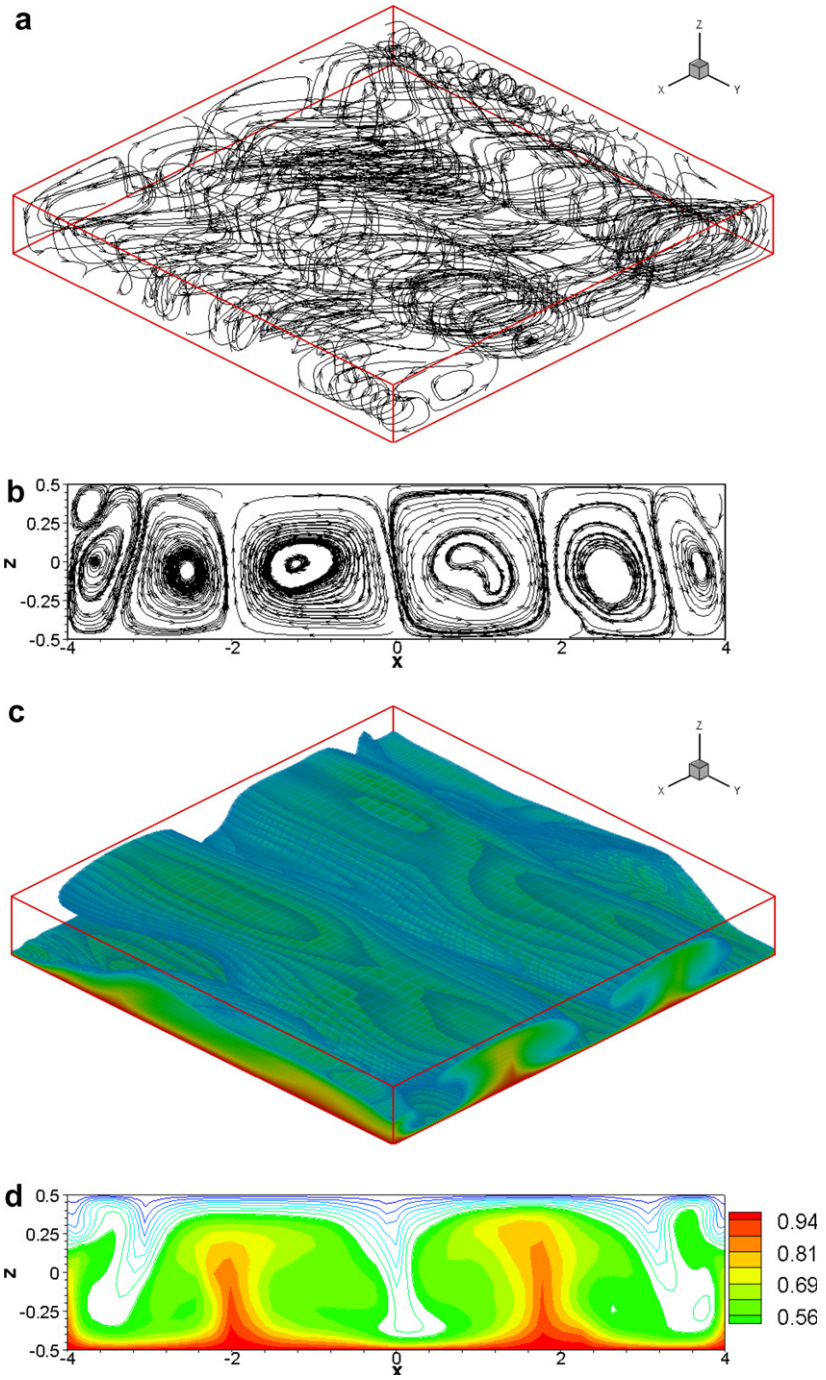

Fig. 5. Streamline plots of (a) 3D flow structures for $Q < Ta$, $Q_h = 1.21 \times 10^6$ and $Ta = 2.5 \times 10^7$, (b) 2D flow structures in central xz-plane. Isotherms showing (c) 3D thermal structures and (d) 2D thermal structures in central xz-plane.

having its axis aligned parallel to the axis of rotation (see Fig. 6a). The two-dimensional section of the same in the horizontal xy-plane shows a large circular rotating roll with four-small rolls near the corners (see Fig. 6b). The thermal flow field as shown in Fig. 6c again depicts a large ascending thermal structure possibly formed due to strong circulation in the enclosure. It is observed that the effect of centrifugal buoyancy is insignificant till $Ta < 2.5^7$ and only at $Ta = 10^{10}$, Ra_w becomes equal to 10^7 and hence comparable to Ra. The effect of centrifugal buoyancy is then to generate or induce a strong large-scale circulation accompanied with strong Ekman pumping as is observed in Fig. 6b and c. These findings are also in consonance with rotating convection results of Hart and Ohlsen [12] and Hart et al. [13] at high Taylor numbers.

4.2. Statistical flow analysis

The statistical analysis is a good tool to represent the turbulence in the fluid flow. Statistical mean and first-

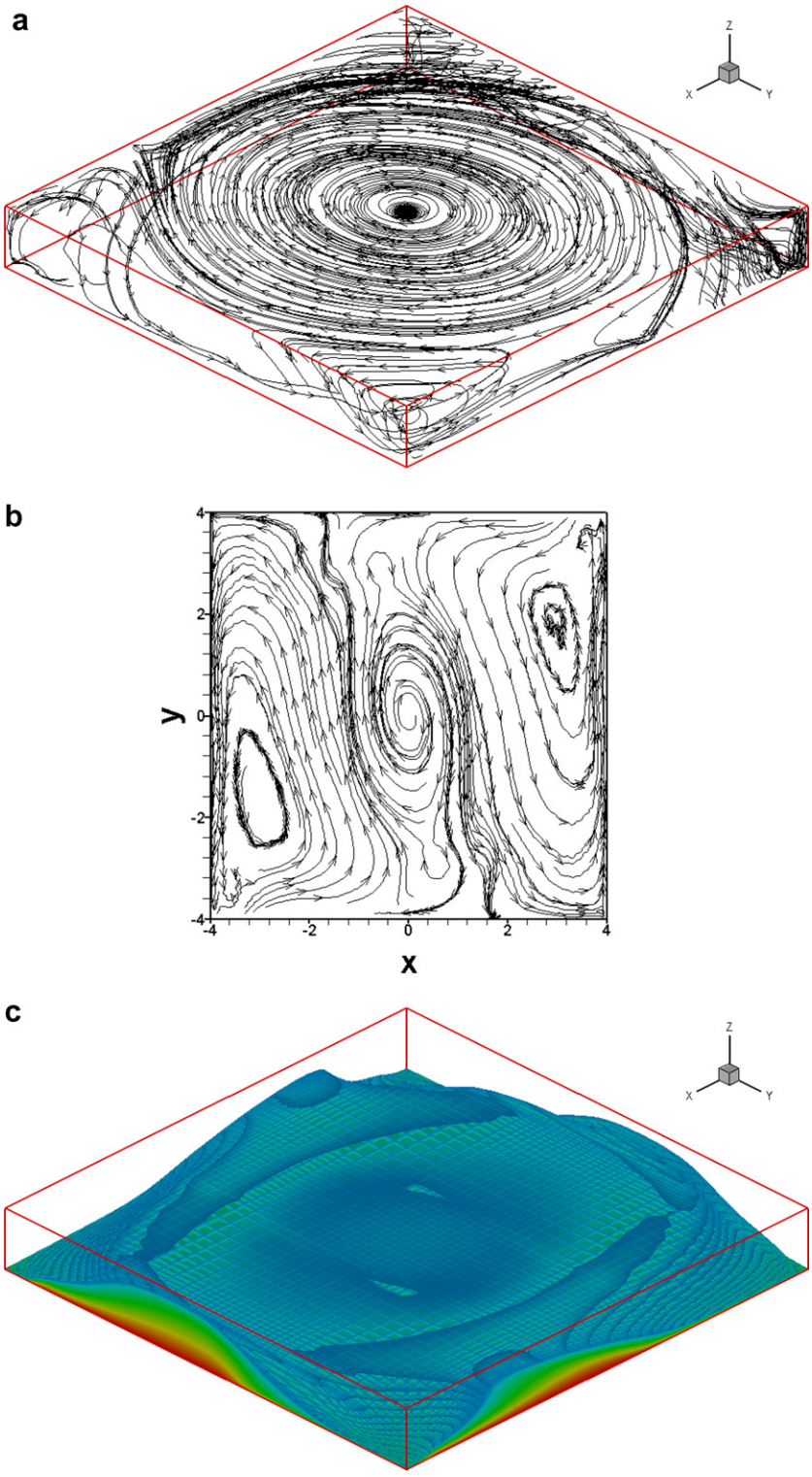

Fig. 6. Streamline plots of (a) 3D flow structures for $Q \ll Ta$, $Q_h = 1.21 \times 10^6$ and $Ta = 10^{10}$, (b) 2D flow structures in central xy-plane and (c) isotherms showing 3D thermal structures.

order moments of all the dynamical variables has been obtained after spatial-averaging over horizontal planes and then time-averaging for a sufficiently long-time till statistically stationary state is achieved. The plots drawn shows the variation of mean and rms values in the inhomogeneous vertical direction for all the cases of numerical simulation.

Fig. 7a and b shows the variation of mean velocity for the case $Q > Ta$ with increasing value of Q at constant Ta. At lower magnetic field ($Q_l = 5.0625 \times 10^4$), all

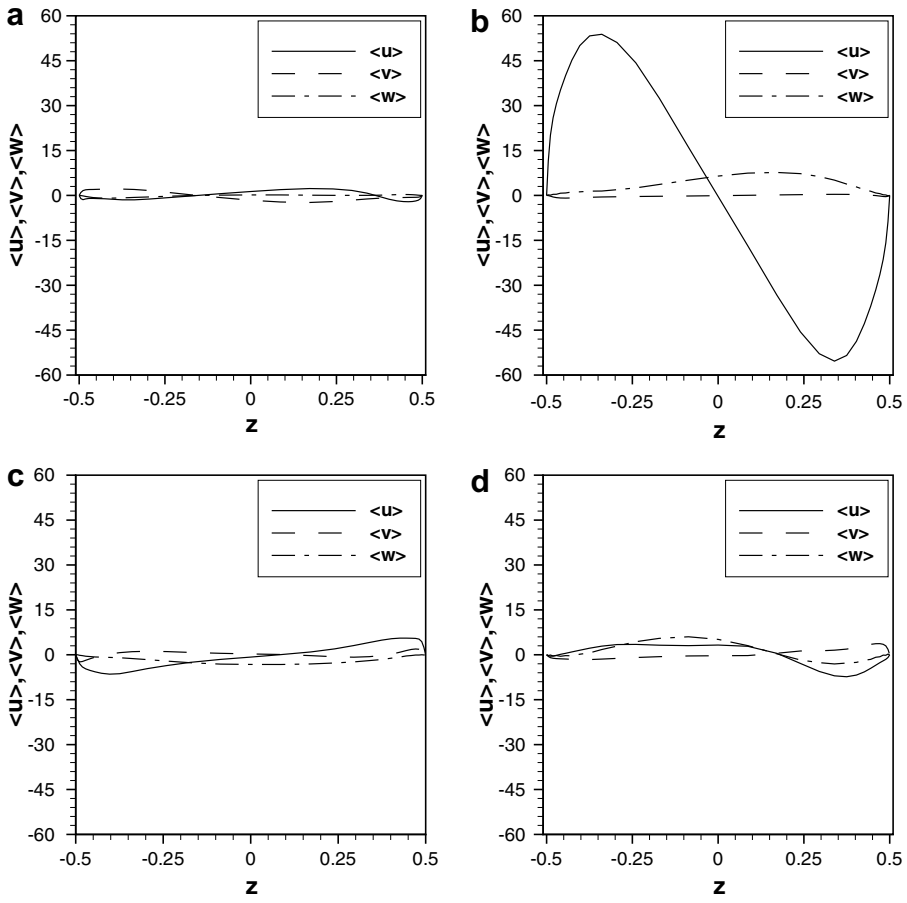

Fig. 7. Variation of the mean velocities $\overline{u}$, $\overline{v}$ and $\overline{w}$ at $Ra = 10^7$: (a, b) for $Q > Ta$, with (a) at $Q_l = 5.0625 \times 10^4$ and $Ta = 0$ and (b) at $Q_h = 1.21 \times 10^6$ and $Ta = 0$, and (c, d) For $Q < Ta$, with (c) at $Q_l = 5.0625 \times 10^4$ and $Ta = 2.5 \times 10^7$ and (d) at $Q_h = 1.21 \times 10^6$ and $Ta = 2.5 \times 10^7$.

velocity component are of comparable magnitude, while at higher magnetic field ($Q_h = 1.21 \times 10^6$) the horizontal mean velocity $\overline{u}$ or $<u>$ shows an anti-symmetric profile about a zero-mean. The transverse mean velocity $\overline{v}$ or $<v>$ has negligibly small values due to magnetic field applied in the same direction and the flow becomes almost two-dimensional in x–z plane. On further increasing Ta corresponding to ($Q < Ta$), the magnitude of all the velocity components show a small variation about a zero-mean.

Fig. 8 shows the variation of rms velocities in the inhomogeneous direction between top and bottom walls of the cavity. As the applied magnetic field is in the transverse direction, the Lorentz force $\mathbf{j} \times \mathbf{B}$ components are larger in the perpendicular directions, i.e. in x- and z-direction and have anisotropic damping effects due to which unequal variation of u_{rms}, v_{rms} and w_{rms} are observed in wall-normal direction. For the case $Q > Ta$, $Q_l = 5.0625 \times 10^4$ and $Ta = 0$ (see Fig. 8a), the u_{rms} is suppressed less by induced Lorentz force as compared to v_{rms} especially near the horizontal walls. In the bulk flow region both the horizontal rms velocity components are of comparable magnitude while the vertical rms velocity component is less affected in this region. On increasing the strength of the magnetic field ($Q_h = 1.21 \times 10^6$) at constant Ta (see Fig. 8b), the rms velocity components in the x- and z- direction increase to a considerable magnitude while the v_{rms} is suppressed almost four times.

At $Q \simeq Ta$ (see Fig. 8c), the behavior is same as in previous plots except the magnitude of vertical velocity w is slightly larger. For $Q < Ta$, i.e. $Q_l = 5.0625 \times 10^4$ and $Ta = 2.5 \times 10^7$, the Coriolis force dominates the flow characteristics. There is significant drop in u_{rms} and w_{rms} due to Coriolis forces, while v_{rms} shows a significant jump. This phenomenon implies that anisotropy induced two-dimensionality of the previous cases gets broken up and the flow field becomes three-dimensional. On increasing the magnetic field further ($Q_h = 1.21 \times 10^6$ and $Ta = 2.5 \times 10^7$), the u_{rms} and w_{rms} increase again while v_{rms} decreases, thus implying that flow is reverting back to anisotropy induced two-dimensional flow (see Fig. 8d and e).

The mean temperature $\overline{\Theta}$ profile shown in Fig. 9a exhibits its formation of thermal boundary layers near the solid walls. The thickness of the thermal boundary layer near the bottom wall increases as we increase the strength of magnetic field though near the top-wall the thickness decreases leading to higher thermal-gradients. The thermal gradients are more influenced by the magnetic field than by

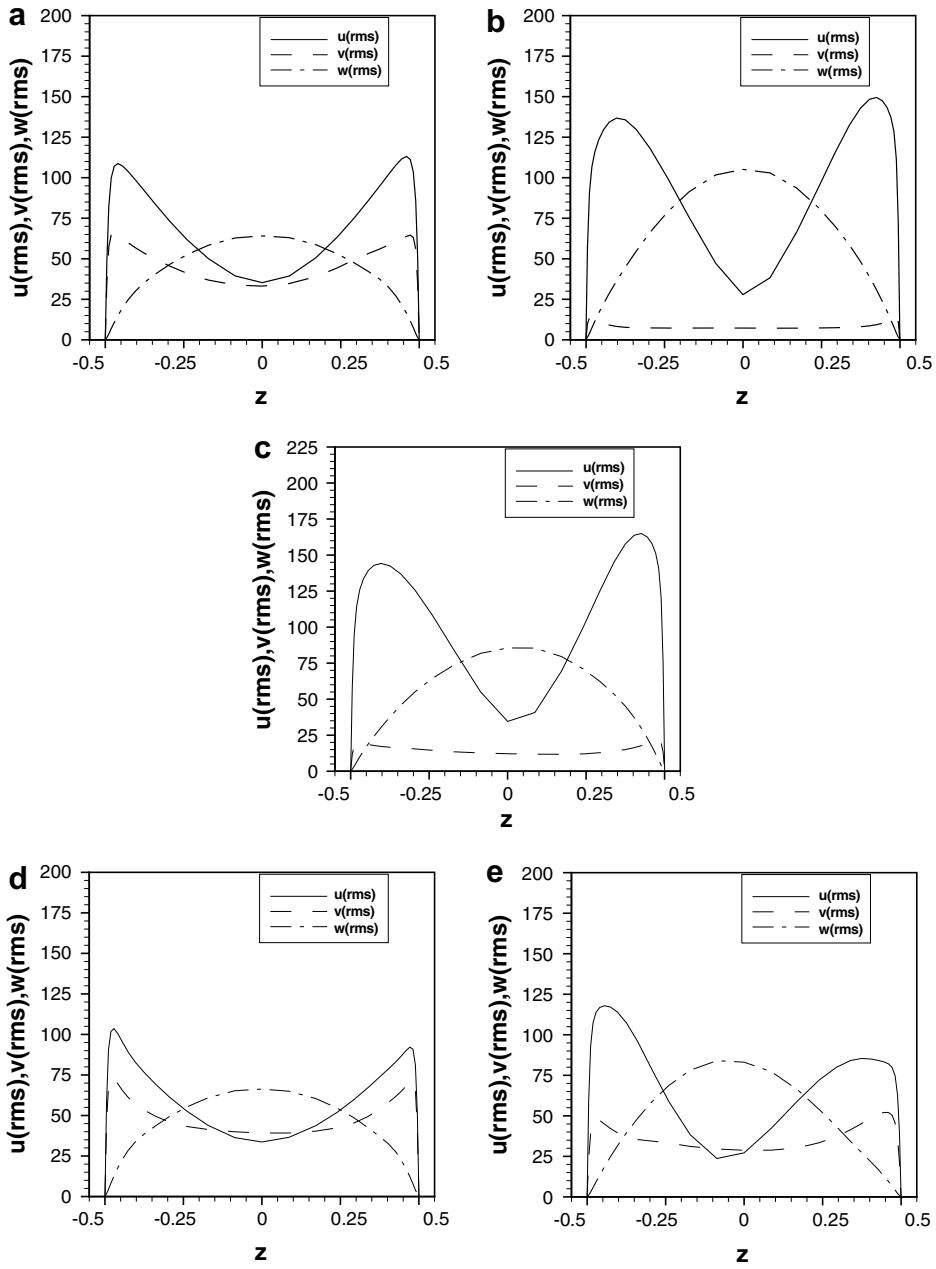

Fig. 8. Variation of the root-mean-square velocities u_{rms}, v_{rms} and w_{rms} at $Ra = 10^7$: (a, b) for $Q > Ta$, with (a) at $Q_l = 5.0625 \times 10^4$ and $Ta = 0$ and (b) at $Q_h = 1.21 \times 10^6$ and $Ta = 0$, (c) For $Q \simeq Ta$, $Q_h = 1.21 \times 10^6$ and $Ta = 10^6$, and (d, e) for $Q < Ta$, with (d) at $Q_l = 5.0625 \times 10^4$ and $Ta = 2.5 \times 10^7$ and (e) at $Q_h = 1.21 \times 10^6$ and $Ta = 2.5 \times 10^7$.

the rate-of-rotation. The rms values for the temperature in Fig. 9b show increasing magnitude of fluctuations with increase in rate-of-rotation. While on the other hand increasing magnetic field strength results in decrease of fluctuations. High gradients of fluctuations are obtained within the near-wall thermal boundary layers for all the cases while in the bulk-flow region Θ_{rms} decreases till the central plane ($z = 0$). These results suggest that with increase of rotation the turbulence becomes more stronger in the whole enclosure while increase of magnetic field reduces turbulent thermal fluctuations.

4.3. Heat transfer analysis

To analyse the simultaneous effect of rotation and transverse magnetic field on heat transfer, we computed variation of space-averaged Nusselt number with time at both the hot and cold walls. For non-rotating cases at $Q > Ta$, from lower to higher values of Q there is a small rise in magnitude of convective heat transfer, i.e. Nusselt number with increasing magnetic field as shown in Fig. 10a and b. This is most likely due to enhanced transport of heat on formation of two-dimensional

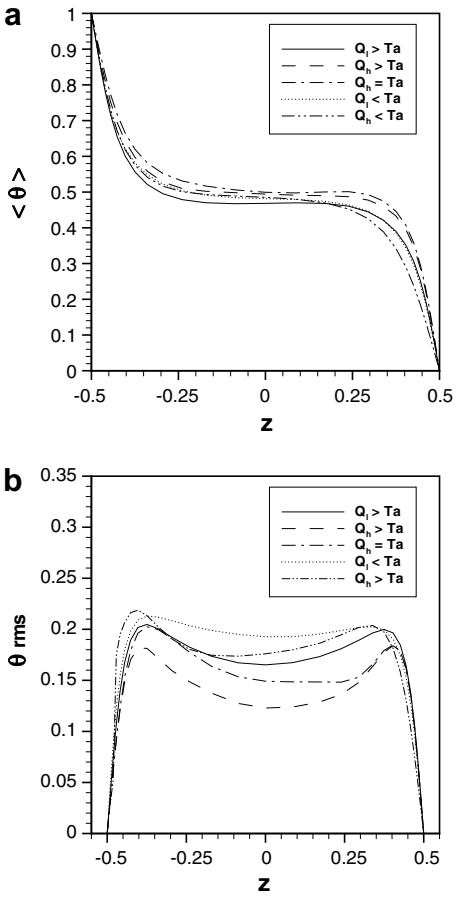

Fig. 9. Variation of (a) mean temperatures $\overline{\Theta}$, (b) root-mean-square temperatures Θ_{rms} for Q_l, $Q_h > Ta$, $Q_h \simeq Ta$ and Q_l, $Q_h < Ta$.

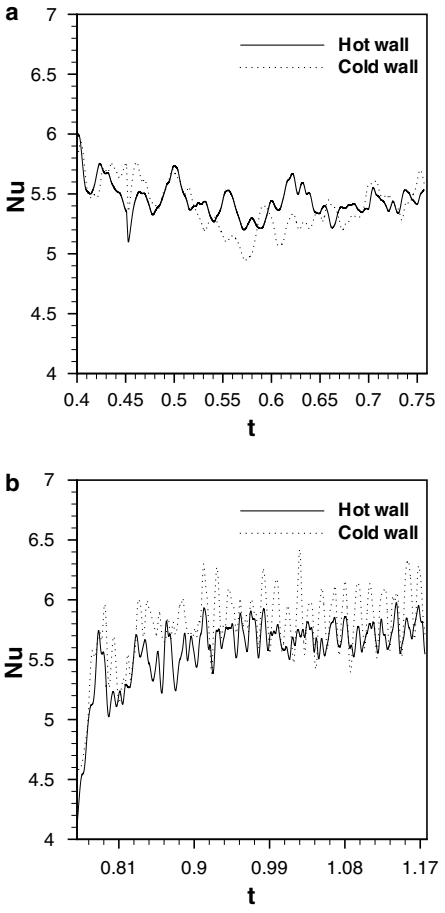

Fig. 10. Variation of Nusselt number, (a, b) For $Q > Ta$, with (a) at $Q_l = 5.0625 \times 10^4$ and $Ta = 0$ and (b) at $Q_h = 1.21 \times 10^6$ and $Ta = 0$.

coherent structures (as seen in Fig. 3a and b) aligned along the direction of applied magnetic field. This result also supports the view of Lehnert and Little [1] that transverse magnetic field do not suppress convection and may even augment it. For the cases $Q_l = 5.0625 \times 10^4$ and $Q_h = 1.21 \times 10^6$ at $Ta = 10^6$, i.e. $Q \simeq Ta$, Fig. 11a and b shows a slight increase in convective heat transfer accompanied with larger fluctuations with the increasing magnetic field. This is again due to formation of aligned two-dimensional coherent structures at higher magnetic field which promote enhanced vertical heat transport.

On further increasing Ta such that $Q < Ta$, i.e. at $Q_l = 5.0625 \times 10^4$ and $Q_h = 1.21 \times 10^6$ at $Ta = 2.5 \times 10^7$, the convective heat transfer compared to the previous low-rotation cases decrease due to enhanced Coriolis forces but there is slight augmentation with increasing magnetic field at same Ta as can be seen in Fig. 11c and d. For both lower and higher magnetic field strengths at highest rotation rate $Ta = 10^{10}$, the convection is suppressed considerably compared to the previous case due to large magnitude of Coriolis forces and moreover the fluctuations vanish leading to a steady-state convection as can be seen in Fig. 11e and f.

4.4. Conclusions

Rotating Rayleigh–Bénard convection of an electrically conducting fluid is significantly influenced by a uniform horizontal magnetic field when applied perpendicular to the vertical temperature gradient. The transverse magnetic field tends to produce anisotropy in the flow field and at sufficiently higher magnetic field strength $Q_h = 1.21 \times 10^6$ there is formation of two-dimensional coherent structures elongated in the direction of magnetic field. This phenomenon of anisotropy induced two-dimensionality is maintained up-till a rotation rate such that $Q \simeq Ta$, while further increase in rotation breaks up two-dimensionality due to enhanced circulation which distorts the alignment of rolls. Further increase in rotation, results in large-scale circulation which leads to formation of a cylindrical rotating fluid column aligned parallel to the rotation axis in consonance with Taylor–Proudman theorem. The induced Lorentz force occurs spatially such that v_{rms} gets suppressed considerably more on increasing strength of applied magnetic field. This leads to strong two-dimensionality generating higher w_{rms} and u_{rms} velocities. The convective heat transfer increases slightly with increase in transverse magnetic field due to formation of heat trans-

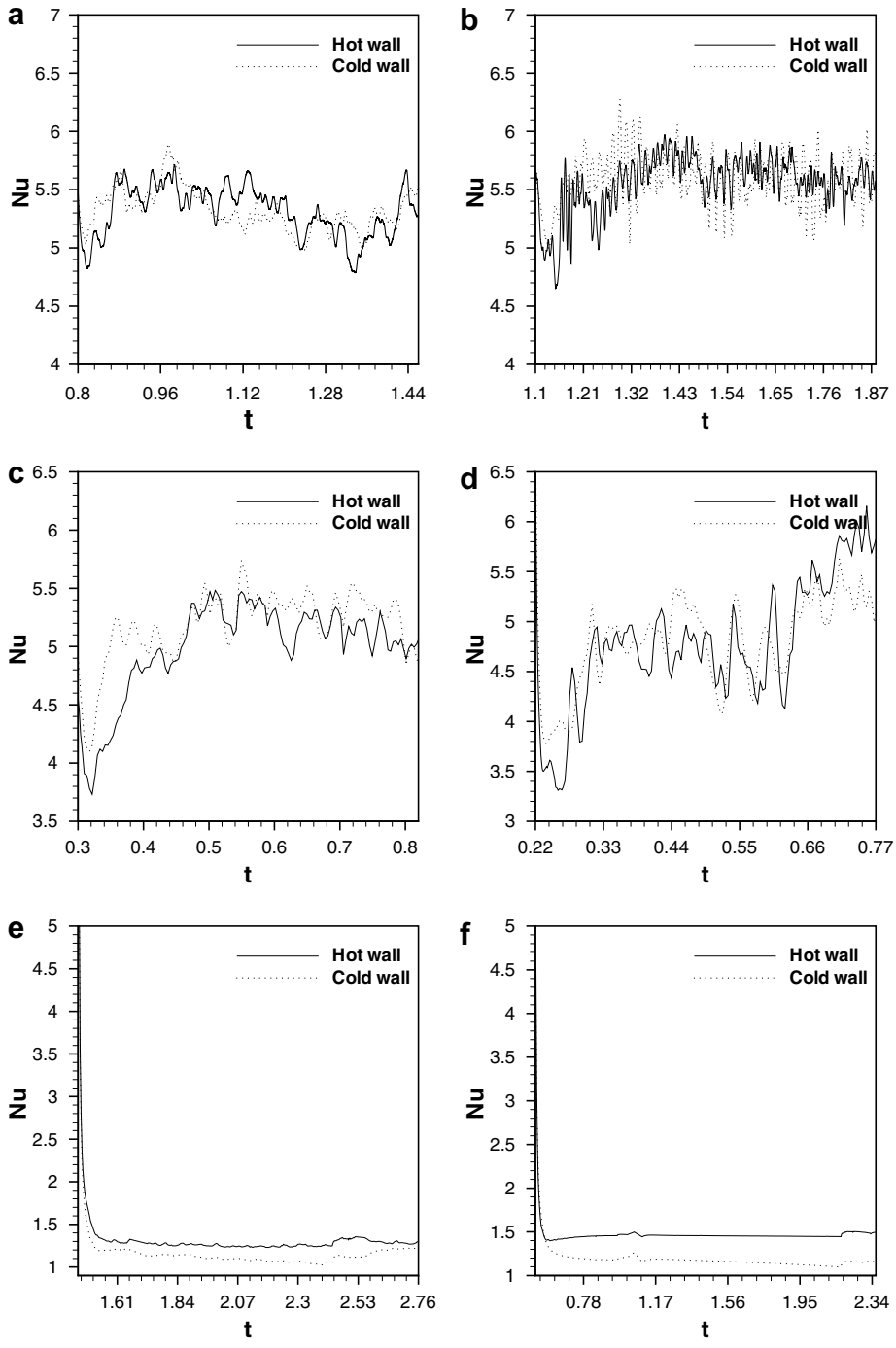

Fig. 11. Variation of Nusselt number: (a) for $Q > Ta$, with (a) at $Q_l = 5.0625 \times 10^4$ and $Ta = 10^6$ and (b) for $Q \simeq Ta$ at $Q_h = 1.21 \times 10^6$ and $Ta = 10^6$, (c) for $Q < Ta$, $Q_l = 5.0625 \times 10^4$ and $Ta = 2.5 \times 10^7$, (d) for $Q < Ta$, $Q_h = 1.21 \times 10^6$ and $Ta = 2.5 \times 10^7$ and (e, f) for $Q \ll Ta$, with (e) at $Q_l = 5.0625 \times 10^4$ and $Ta = 10^{10}$ and (f) at $Q_h = 1.21 \times 10^6$ and $Ta = 10^{10}$.

port enhancing coherent structures till $Q \simeq Ta$. It is observed that increase of rotation suppresses the convection due to enhanced Coriolis forces.

References

[1] L. Lehnert, N.C. Little, Experiments on the effect of inhomogeneity and obliquity of a magnetic field in inhibiting convection, Tellus 9 (1957) 97–103.

[2] H. Ozoe, K. Okada, The effect of the direction of the external magnetic field on the three-dimensional natural convection in a cubical enclosure, Int. J. Heat Mass Transfer 32 (1989) 1939–1954.

[3] A. Juel, T. Mullin, H. Ben Hadid, D. Henry, Magnetohydrodynamic convection in molten gallium, J. Fluid Mech. 378 (1998) 97–118.

[4] H. Ben Hadid, D. Henry, Numerical study of convection in the horizontal Bridgman configuration under the action of a constant magnetic field. Part 2. Three-dimensional flow, J. Fluid Mech. 333 (1997) 57–83.

[5] J.M. Aurnou, P.L. Olson, Experiments on Rayleigh–Bénard convection, magnetoconvection and rotating magnetoconvection in liquid gallium, J. Fluid Mech. 430 (2001) 283–307.
[6] U. Burr, U. Muller, Rayleigh–Bénard convection in liquid metal layers under the influence of a horizontal magnetic field, J. Fluid Mech. 453 (2002) 345–369.
[7] T.E. Faber, Fluid Dynamics for Physicists, Cambridge University Press, 1995 (Chapter 9) pp. 378–383..
[8] D.J. Tritton, Physical Fluid Dynamics, Van Nostrand Reinhold, UK, 1982.
[9] S. Chandrasekhar, Hydrodynamic and Hydromagnetic Stability, Dover, 1981.
[10] N. Hasan, M.F. Baig, Evolution to Aperiodic Penetrative Convection in Odd Shaped Rectangular Enclosures, Int. J. Numer. Meth. Heat Fluid Flow 12 (2002) 895–915.
[11] T.L. Lee, T.F. Lin, Transient three-dimensional convection of air in a differentially heated rotating cubic cavity, Int. J. Heat Mass transfer 39 (1996) 1243–1255.
[12] J.E. Hart, D.R. Ohlsen, On the thermal offset in turbulent rotating convection, Phys. Fluids 11 (8) (1999).
[13] J.E. Hart, S. Kittelman, D.R. Ohlsen, Mean flow precession and temperature probability density functions in turbulent rotating convection, Phys. Fluids 14 (3) (2002).